LA-UR-21-30730
Accepted Manuscript

A robust three-parameter reference curve for condensed phase materials

Lozano Sanchez, Jose Eduardo
Aslam, Tariq Dennis

To be published in: Journal of Applied Physics

DOI to publisher's version: 10.1063/5.0076897

Permalink to record:
http://permalink.lanl.gov/object/view?what=info:lanl-repo/lareport/LA-UR-21-30730

A robust three-parameter reference curve for condensed phase materials

Eduardo Lozano[a)] and Tariq D. Aslam
Physics and Chemistry of Materials (T-1), Los Alamos National Laboratory, Los Alamos, NM 87545, USA

(Dated: 8 December 2021)

Many isothermal equations of state lead to numerical problems under tension conditions due to negative bulk modulus. We summarize the properties of four existing models and devise a continuous non-piecewise reference curve to address this issue. The final functional form contains three fitting parameters that are directly related to the bulk modulus and its pressure derivative at the reference state and at infinite pressures. We also include bounds that guarantee the monotonicity of its pressure derivative in all volume space. To demonstrate the qualitative features of each isotherm, we conduct calibrations against experimental data for cyclotetramethylene tetranitramine (HMX), magnesium oxide (MgO), gold (Au), and platinum (Pt). Pressure residuals and root mean square deviations show that the proposed functional form is capable of adequately fitting the data compared to other three-parameter models.

I. INTRODUCTION

Modeling the high-pressure response of substances is central to multiple fields including geophysics, astrophysics, aerospace, and high explosives (HEs). Continuum hydrodynamic calculations can be used to simulate practical applications where the thermodynamic properties of the materials are described by an equation of state (EOS).

Empirical high-pressure models base the full EOS on a reference curve which can be a Hugoniot, an isentrope, or an isotherm. Hugoniots as a reference are able to fit shock data in a simple fashion but they will become ill-posed outside a certain density range[1]. Isentropes are the preferred choice when dealing with incomplete EOSs since they offer a relatively robust and wide sampling of phase space without knowledge of specific heats. However, they can potentially contain regions of thermodynamic instability due to negative isothermal and/or isentropic bulk moduli. The same issue occurs with reference isotherms which typically become problematic at low temperatures and high specific volumes.

To be able to construct a complete or incomplete equation of state, a mathematical description of the reference curve is needed. Reference isotherms are usually expressed as $P = P(V)$ with P being the thermodynamic pressure and V the specific volume. The functional forms also contain a number of free parameters that are calibrated using experimental data or density functional theory[2]. These parameters are often related to physical thermodynamic properties such as the bulk modulus $K = -V\mathrm{d}P/\mathrm{d}V$ and its derivative with respect to pressure $K' = \mathrm{d}K/\mathrm{d}P$.

There are many two-parameter and three-parameter analytic isotherms reported in the literature[3]. Three popular functional forms are the Birch-Murnaghan[4], the Rose-Vinet[5], and the Keane[6]. These three forms provide an accurate representation of condensed-phase materials over an existing range of isothermal compression data but their mathematical properties can lead to stability problems under tension. Solids and liquids can go into expanded states where the material will eventually fail under certain tensile loading conditions (spallation/cavitation). Failure models, such as Rajendran-Dietenberger-Grove (RDG)[7] or tensile plasticity (TEPLA)[8], aim to capture the dynamic deformation of ductile materials and include a rate-dependent law for the nucleation and growth of voids. Under an arbitrary amount of expansion, the reference curve must remain qualitatively correct prior to the appearance of those voids. If the material enters a region where the EOS has unphysical properties—e.g., negative compressibility—the simulation will break down.

To address this problem, most reactive flow models for high explosives use reference curves defined by piecewise functions with multiple branches. For instance, the Wescott-Stewart-Davis (WSD)[9] and Arrhenius WSD (AWSD)[10] models use the *Davis reactants* EOS[11,12] which is based on a piecewise reference isentrope that guarantees positivity of the sound speed[13]. Whitworth and Lambourn[14] also use a piecewise reference isentrope. Menikoff[15] fits the kinks in isothermal data for triaminotrinitrobenzene (TATB) using a Keane form with two separate set of parameters. Velizhanin and Coe[16] use a piecewise cold curve by combining the Birch-Murnaghan in compression ($V \leq V_0$) and the Lennard-Jones in expansion ($V > V_0$). These functions can be designed carefully to be continuous differentiable everywhere and avoid the appearance of nonphysical states. However, having multiple branches will always result in a more intricate algebra, slower computations, and more extensive verification.

The goal in this work is to derive a robust three-parameter non-piecewise functional form that remains strictly well-behaved in all volume space and with enough flexibility to fit isothermal compression data. The energy term from integrating $P(V)$ must also be analytic with each fitting parameter being related to the bulk modulus and its derivative with respect to pressure.

The structure of this manuscript is described next. Section II summarizes the properties of four popular functional forms, namely Birch-Murnaghan[4], Rose-Vinet[5], Keane[6], and Davis[9,11]. Section III presents the derivation of a three-parameter reference curve along with its properties. To demonstrate the qualitative features of each isotherm, several calibrations against experimental data for cyclotetramethylene tetranitramine (HMX), magnesium oxide (MgO), gold (Au), and platinum (Pt) are given in Section IV. Section V summarizes the conclusions and possible avenues for future work.

[a)] Electronic mail: lozano@lanl.gov

Relevant thermodynamic relations and reference curve parameters are given in Appendices A and B.

II. REVIEW OF EXISTING REFERENCE CURVES

In high-pressure applications, infinitesimal strain theories break down and elastic moduli becomes a strong function of pressure. Such behavior has driven a large body of work in the subject of isothermal equations of state[3,17]. The main characteristics of each functional form are revealed by the bulk modulus K and its derivative with respect to pressure K'. Their value at the reference state (K_0, K_0') and at infinite pressures (K_∞') determine the fit to experimental data. In the following sections, the subscript "0" will be used to represent the reference state at zero pressure, the subscript "∞" indicate infinite pressures, and $\eta = V/V_0$ is the expansion ratio with V_0 being the reference specific volume.

The behavior as $P \to \infty$ constitutes an important qualitative aspect of the model that is subject to thermodynamic constraints. Some authors[18,19] suggest that K_∞' is defined by the Thomas-Fermi theory ($K_\infty' = 5/3$), while others[6,20] argue that it should be a property dependent on the material. Using thermodynamic arguments, Stacey and Davis[20] propose two minimum conditions for a solid EOS: (i) $5/3 < K_\infty' < \infty$, (ii) $P > 0$ and $K > 0$ over the entire compression range ($\eta < 1$). The first condition is related to the assertion $K_\infty' = (P/K)_\infty$, which simply states that the bulk modulus becomes linear in pressure in the infinite pressure limit. Additional constraints on the gradient of $(1/K')$ versus (P/K) at infinite pressures have been proposed more recently by Stacey and Hodgkinson[21].

Apart from these conditions, we will analyze the response over the expansion range ($\eta > 1$). This regime has not received the same degree of attention but a correct qualitative behavior in expansion is arguably as important as the infinite pressure limit. Specifically, thermodynamic stability requires the bulk modulus to remain positive for all $V > 0$. The implications of such stability constraint become apparent when conducting hydrodynamic calculations. Using a convex EOS and neglecting any material strength, a rarefaction wave propagates at the characteristic velocity $u \pm c$, where u is the particle velocity and c is the isentropic sound speed. If the EOS enters a region where the isentropic bulk modulus is negative, the sound speed becomes an imaginary number causing numerical instability due to the loss of hyperbolicity of the governing equations. We will now analyze the main characteristics of four commonly utilized reference curves: the third-order Birch-Murnaghan[4], the Rose-Vinet[5], the Keane[6], and the Davis[11,12] forms.

A. Birch-Murnaghan

Birch[4] defined the Helmholtz free energy as a n-th order polynomial expansion in terms of the Eulerian finite strain ε. Truncating the terms beyond $\mathscr{O}(\varepsilon^4)$ and differentiating with respect to the specific volume V at constant temperature T provides an expression for $P(V)$. The polynomial coefficients in the expansion are determined in terms of the isothermal bulk modulus at the reference state K_0 and its derivative with respect to pressure K_0'. These steps result in the third-order Birch-Murnaghan:

$$\begin{aligned} P_{\text{birch}}(\eta) =& \frac{3}{2} K_0 \left(\eta^{-\frac{7}{3}} - \eta^{-\frac{5}{3}}\right) \\ & \times \left[1 + \frac{3}{4}\left(K_0' - 4\right)\left(\eta^{-\frac{2}{3}} - 1\right)\right]. \end{aligned} \tag{1}$$

The two parameters that control the shape of the curve, namely K_0 and K_0', are material properties defined at the reference state. At high pressures, Eq. (1) satisfies the algebraic constraint $K_\infty' = (P/K)_\infty$ with a limit $K_\infty' = 3$ identical for all materials. The Birch-Murhaghan isotherm leads to a concave downward principal Hugoniot locus in the shock velocity (U_s) versus particle velocity (u_p) plane[22]. This feature is characteristic of molecular crystals, amorphous solids, and liquids[1]. Despite satisfying the thermodynamic bound $K_\infty' > 5/3$, the functional form in Eq. (1) displays an anomalous behavior for $K_0' < 4$ with negative pressure values at high compression. Additionally, the K' function is not strictly decreasing in compression for $K_0' \in (4, 14/3)$ resulting in the appearance of an inflection point in the K-P curve.

In expansion, the third-order Birch-Murnaghan is not a strictly decreasing function of η which leads to unphysical regions of negative compressibility independently of the calibration for K_0 and K_0'. It is useful to identify these regions for practical applications. The bulk modulus can be written in closed-form as

$$\begin{aligned} K_{\text{birch}}(\eta) =& \frac{1}{8} K_0 \eta^{-3} \Big[27(K_0' - 4) \\ & - 14\eta^{\frac{2}{3}}(3K_0' - 14) + 5\eta^{\frac{4}{3}}(3K_0' - 16)\Big], \end{aligned} \tag{2}$$

which has two roots η_1^* and η_2^* in the $\eta > 0$ and $K_0' > 0$ quadrant. Fig. 1 shows the value of each one of them as a function

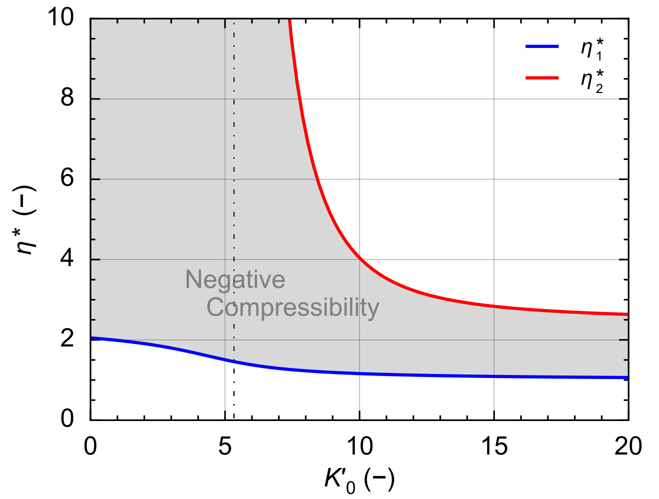

FIG. 1. Regions in the $\eta = V/V_0$ domain with negative bulk modulus (gray area) for the Birch-Murnaghan based on the value of K_0'. The dash-dotted line marks the location of a vertical asymptote for η_2^*

of K_0'. Note from Eq. (2) that η_1^* and η_2^* are independent of K_0 since it multiplies the entire right hand side. From the definition of the bulk modulus, these roots mark the location of local extrema in $P(\eta)$. That is, η_1^* correspond to a local pressure minimum and η_2^* to a local pressure maximum. For any K_0' at expansion ratios larger than η_1^*, the bulk modulus becomes negative. The domain of the second root η_2^* is marked by a vertical asymptote at $K_0' = 16/3$. If $K_0' > 16/3$, η_2^* is real-valued and the bulk modulus becomes positive again at expansions $\eta > \eta_2^*$. The third-order Birch-Murnaghan also loses convexity past η_1^* where $K' < -1$ (see Appendix A).

B. Rose-Vinet

Rose et al.[23] proposed a potential function for the binding energy in metals as a function of the interatomic distance. The authors[24] then found such relation to be also representative of other materials and they utilize it to derive an algebraic expression for the pressure as a function of the specific volume. Using the thermodynamic definition of the bulk modulus, the atomic spacing can be replaced in favor of K_0 and K_0' resulting in the Rose-Vinet isotherm[5]:

$$P_{\text{vinet}}(\eta) = 3K_0\eta^{-\frac{2}{3}}\left(1-\eta^{\frac{1}{3}}\right) \times \exp\left[\frac{3}{2}\left(K_0'-1\right)\left(1-\eta^{\frac{1}{3}}\right)\right]. \quad (3)$$

Despite being credited to Vinet et al.[5,24], Eq. (3) was first presented by Stacey and co-workers[17] who derived it directly from the alternative form of the Morse potential[25] proposed by Rydberg[26]. The Rose-Vinet is also a two-parameter isotherm where the shape of the function is governed by the bulk modulus and its pressure derivative at the reference state. Similar to Eq. (1), it satisfies the algebraic constraint $K_\infty' = (P/K)_\infty$ but with an asymptotic value $K_\infty' = 2/3$. This value is below the lower thermodynamic bound for K_∞' derived by Stacey[20]. Hama and Suito[27] and Holzapfel[28] modified the original form to render the Thomas-Fermi limit. But this change affects the Helmholtz free energy at $T = 0$ which can no longer be written in closed-form.

The expansion characteristics of Eq. (3) are better understood by analyzing the bulk modulus,

$$K_{\text{vinet}}(\eta) = \frac{1}{2}K_0\left[4\eta^{-\frac{2}{3}} + \eta^{-\frac{1}{3}}(3K_0'-5) - 3(K_0'-1)\right]\exp\left[\frac{3}{2}\left(K_0'-1\right)\left(1-\eta^{\frac{1}{3}}\right)\right]. \quad (4)$$

Eq. (4) contains a single root η^* in the $\eta > 0$ and $K_0' > 0$ quadrant. The location of the root in K_0' space is shown in Fig. 2. At unphysically small K_0' values, η^* is complex and the Rose-Vinet isotherm has a positive bulk modulus for all $V > 0$. For $K_0' \gtrsim 0.9$, the root takes a real value with $\lim_{K_0'\to\infty} \eta^*(K_0') = 1$ which results in an unphysical behavior at finite compression ratios. Similar to the Birch-Murnaghan, one can expect the Rose-Vinet to cause numerical problems in the presence of relatively weak rarefaction waves.

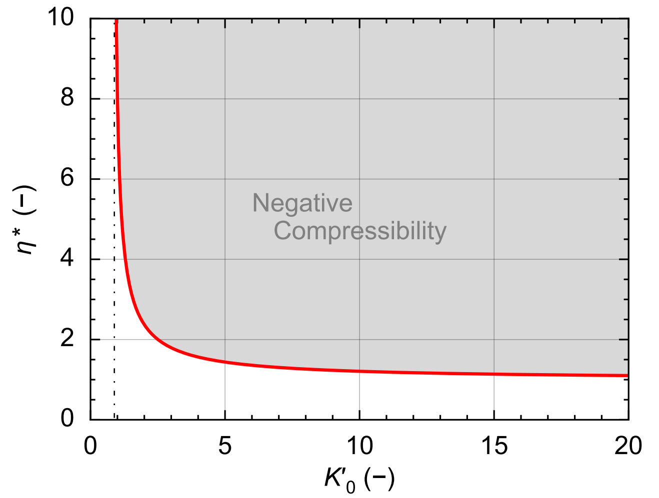

FIG. 2. Regions in the $\eta = V/V_0$ domain with negative bulk modulus (gray area) for the Rose-Vinet based on the value of K_0'. The dash-dotted line marks the location of a vertical asymptote for η^*

C. Keane

Keane[6] assumes that the pressure can be written as a n-th order polynomial expansion of the strain ε. For $n = 2$, the author suggests that the quadratic and linear coefficients are linearly dependent on each other resulting in an analytic K'-K relation: $K' = K_\infty' + (K_0' - K_\infty')K_0/K$. Such relation is parameterized not only by K_0 and K_0' but also K_∞'. Upon integration, the Keane form can be written as:

$$P_{\text{keane}}(\eta) = K_0\left[\frac{K_0'}{K_\infty'^2}\left(\eta^{-K_\infty'}-1\right) + \left(\frac{K_0'}{K_\infty'}-1\right)\ln(\eta)\right]. \quad (5)$$

A notable feature of Eq. (5) is that one recovers the classic Murnaghan isotherm[29] for $K_\infty' = K_0'$. The Keane isotherm is a three-parameter reference curve and is credited to be the first one that recognizes the importance of the infinite pressure limit[20]. Eq. (5) satisfies the linear algebraic constraint $K_\infty' = (P/K)_\infty$ although the infinite pressure value is now material-dependent. Using a simple potential function[30], Keane[6] provides upper and lower bounds for the K_∞' parameter but these have been the subject of a later revision[31]. K_∞' is generally left as a free parameter in fitting high-pressure data. Alternatively, Stacey et al.[17] provides an expression for K_∞' in terms of K_0, K_0' and K_0''.

Integrating the original K'-K relation with respect to the compression ratio yields a simple expression for the bulk modulus,

$$K_{\text{keane}}(\eta) = K_0\left[\frac{K_0'}{K_\infty'}\left(\eta^{-K_\infty'}-1\right)+1\right]. \quad (6)$$

Eq. (6) contains a single root η^* which is now a function K_0' and K_∞'. Fig. 3 shows a contour plot for η^* such that $K_{\text{keane}}(\eta^*) = 0$ in K_0'-K_∞' space. As indicated by the colorbar, $\eta^* \geq 1$ thus Eq. (6) is expected to be positive for all

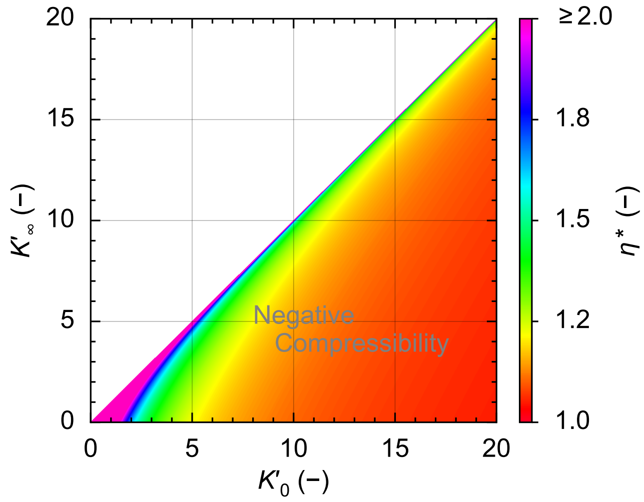

FIG. 3. Left endpoint in the $\eta = V/V_0$ domain (colormap) with negative bulk modulus for the Keane based on K'_0 and K'_∞

compression values ($\eta < 1$). The Keane isotherm would become strictly decreasing with a positive bulk modulus in all $\eta > 0$ if and only if $K'_\infty > K'_0$, i.e., η^* is a complex number. However, high-pressure data shows that K''_0 is negative implying a concave downward K-P curve and $K'_\infty \leq K'_0$. Under that condition, Fig. 3 shows that there is always a limiting η^* value such that the bulk modulus becomes negative and the $P_{\text{keane}}(\eta)$ curve reaches a minimum at finite expansions. Similar to Birch-Murnaghan and Rose-Vine, the Keane isotherm also loses convexity past η^*.

D. Davis

Based on the work of Enig[32], Davis[11,33] derives a reference curve using the Walsh mirror-image approximation[34] and the Riemann relation for the particle velocity on an isentrope. To allow for calibration at high pressures, Stewart et al.[12] replaced the definition of the principal isentrope in compression by a truncated expansion of the original exponential form. The final piecewise form constitutes the reference curve for the WSD[9] and AWSD[10] reactive burn models and can be written as:

$$P_{\text{davis}}(\eta) = \begin{cases} \hat{P}\left[\sum_{j=1}^{3}\frac{(4By)^j}{j!} + C\frac{(4By)^4}{4!} + \frac{y^2}{(1-y)^4}\right], & \eta \leq 1; \\ \hat{P}\left[\exp(4By) - 1\right], & \eta > 1; \end{cases} \tag{7}$$

where $y = 1 - \eta$ and $\hat{P} = A^2/4BV_0$. Both branches in Eq. (7) are continuous at $\eta = 1$ up to y^3 avoiding any problems when computing sound speeds. Eq. (7) contains three fitting parameters A, B, C but only A and B can be related to the bulk modulus and its derivative with respect to pressure: $K_0 = A^2/V_0$, $K'_0 = 4B + 1/2B - 1$. At high pressures, Eq. (7) satisfies the algebraic constraint $K'_\infty = (P/K)_\infty$ with a limit $K'_\infty = 4$ identical for all materials. Despite being derived using isentropic flow arguments—see Appendix A in Davis[11]—the Davis functional form can be utilized to fit isothermal data under a suitable calibration.

The bulk modulus can be derived analytically from Eq. (7) yielding

$$K_{\text{davis}}(\eta) = \begin{cases} \hat{P}(1-y)\left[\sum_{j=1}^{3}\frac{(4B)^j y^{j-1}}{(j-1)!} + C\frac{(4B)^4 y^3}{3!} + \frac{2y(1+y)}{(1-y)^5}\right], & \eta \leq 1; \\ 4\hat{P}B(1-y)\exp(4By), & \eta > 1; \end{cases} \tag{8}$$

which is positive for all $\eta > 0$. Similar to the Murnaghan isotherm, the second branch in Eq. 8 decreases monotonically to zero as $\eta \to \infty$. The bulk modulus K in compression is also monotonic but K' displays an oscillatory behavior with local minima that can go below $5/3$ for certain calibrations. Despite having a non-monotone K', the Davis reference curve remains convex since $K' > -1$ for any realistic A, B, C set. See Appendix A for a discussion on EOS convexity.

III. THREE-PARAMETER REFERENCE CURVE

The four reference curves described in Section II can lead to problems in expansion or contain multiple branches that increase the algorithmic complexity and computational cost. Based on the points described, the objective is to design a robust non-piecewise functional form with: (i) appropriate K-P relation and limit at infinite pressures, (ii) qualitatively correct characteristics in expansion, (iii) flexible enough to fit a wide range of data with variable K_0, K'_0, and K'_∞, and (iv) with a closed-form Helmholtz free energy term at $T = 0$.

A. Derivation

The classical Murnaghan isotherm[29] satisfies some of the above properties but it is only able to reproduce experimental data up to approximately $K_0/2$ in pressure[35]. Along the $T = 0$ isotherm, we can obtain an expression for Helmholtz free energy by integrating the pressure-volume relation,

$$F_{\text{murnaghan}}(\eta) = F_0 + \frac{V_0 K_0}{K'_0 - 1}\left[\frac{\eta}{K'_0}\left(\eta^{-K'_0} - 1\right) + \eta - 1\right]. \tag{9}$$

Eq. (9) contains a power law and a linear term where the latter dominates in the expansion regime. Another functional form with positive bulk modulus everywhere is the Walsh mirror-image[11] that appears in the Davis reference curve for $\eta > 1$. Integrating the second branch of Eq. (7) gives

$$F_{\text{walsh}}(\eta) = F_0 + \frac{A^2}{4B}\left[\frac{\exp(4B(1-\eta)) - 1}{4B} + \eta - 1\right], \tag{10}$$

which also contains a linear term that dominates in expansion. The exponential term in Eq. (10) results in a considerably softer function than the power law in Eq. (9). This generally allows fitting isothermal data more easily but it has the unwanted characteristic of reaching a finite P value as $\eta \to 0$. The goal is to retain some of the features in Eq. (9) and Eq. (10) in a purely mathematical sense by constructing a flexible functional form that remains well-behaved for all $\eta > 0$. Therefore, we suggest the following four-parameter Helmholtz free energy along the cold curve:

$$F(\eta) = F_0 + AV_0 \left[\eta^{-B} \exp\left(\frac{C}{D}(1-\eta^D) \right) + \eta(B+C) - (B+C+1) \right]. \tag{11}$$

The compression regime is described by a power law with an exponential cutoff where the B, C, D parameters control the stiffness of the curve. As the material goes into tension, this term approaches zero and the linear portion takes over. The functional form can be interpreted as the Murnaghan combined with the Walsh mirror-image and it is denoted as the MACAW reference curve.

The change in the bulk modulus with increasing pressure depends on the value of B and D and it is highly unconstrained for the four-parameter model in Eq. (11). Experimental high-pressure data for most materials suggests that K-P is concave downwards, thus we would like to find a relation between B and D such that K' decreases monotonically down to a minimum value K'_∞. Departing from Eq. (11), we can compute analytically the second derivative of the bulk modulus with respect to pressure K'' (see Appendix A). The roots of $K''(\eta)$ indicate the location where K' contains local extrema. We can then use these roots to determine the minimum B as a function of D such that all roots are complex-valued and $K'' < 0$ for all $\eta > 0$. Considering only the physically-relevant $B, D > 0$ quadrant, such relation is given by:

$$B_{\min} = \begin{cases} D, & D < 1; \\ \dfrac{1}{12D^3}\left[D^2(7D^2 - 6D + 3) + \dfrac{1}{\omega}(17D^8 + D^4 - 2D^6) + \omega \right], & D \geq 1; \end{cases} \tag{12}$$

where,

$$\omega = \left(a + 2\sqrt{b}\right)^{1/3},$$
$$a = D^6(71D^6 - 15D^4 + 9D^2 - 1),$$
$$b = D^{14}(32D^4 - 3D^2 + 3)(D^2 - 1)^3.$$

Eq. (12) is indicated by the red piecewise curve in Fig. 4. Any (B,D) point located above $B_{\min}$ guarantees the monotonicity of K' for all $\eta > 0$. Points located below $B_{\min}$ result in a local minimum in K' that falls below K'_∞.

Since the model in Eq. (11) implies that $P \to \infty$ as $\eta \to 0$, we obtain the following relation:

$$K'_\infty \equiv \lim_{\eta \to 0} K'(\eta) = B + 1, \tag{13}$$

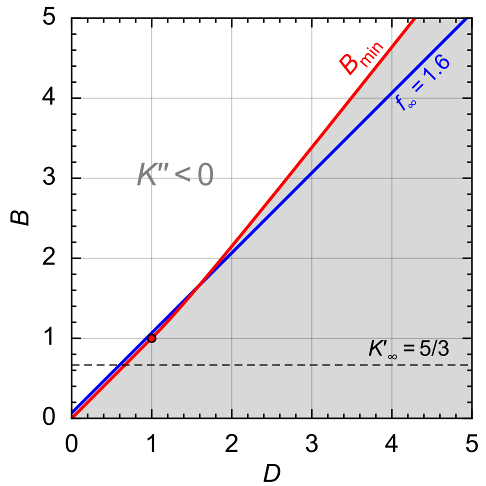

FIG. 4. Minimum B as a function of D that guarantees monotonicity of K' for all $\eta > 0$ (red curve) and limiting value of D for $f_\infty = 1.6$ (blue curve)

where the thermodynamic bound $K'_\infty > 5/3$ then implies that B should always be larger than $2/3$. The parameter D is also related to λ_∞, a relevant derivative of the Grüneisen coefficient Γ at infinite pressures where $\lambda = (\partial \ln q / \ln V)_T$ and $q = (\partial \ln \Gamma / \ln V)_T$ (see Stacey[36]). That is,

$$\lambda_\infty \equiv K'_\infty + \frac{1}{K'_\infty}\left(\frac{KK''}{1 - K'P/K} \right)_\infty = D \quad \forall\ D < K'_\infty. \tag{14}$$

Stacey and Hodgkinson[21] shows that λ_∞ must be positive with a value bounded by the following restriction:

$$\lambda_\infty < K'_\infty - \frac{2}{3} f_\infty, \tag{15}$$

where $f_\infty \in (1.4, 1.8)$ is a parameter that depends on statistical details of atomic thermal vibrations with a range of values that varies between different theories[21]. Given the relation in Eq. (14), the above inequality can be used to impose an additional constraint on B as a function of D. Replacing K'_∞ and λ_∞ in Eq. (15) yields

$$B > D + \frac{2}{3} f_\infty - 1. \tag{16}$$

Since Eq. (16) depends on f_∞ which can vary, we select the midpoint value of the interval ($f_\infty = 1.6$) as an estimator—blue curve in Fig. 4. The intersection point between the red and blue curves can be then used to approximate D. For algebraic simplicity, we set $D = 3/2$ reducing Eq. (11) to a three-parameter model. Substituting $D = 3/2$ in Eq. (12) also provides a lower bound $B \gtrsim 45/29$ that can be applied in the P-V fitting step. The rational number $45/29$ stems from the [2/1] Padé approximant of $B_{\min}$ centered at $D = 1$ and evaluated at $D = 3/2$. These values generally provide enough flexibility to fit a wide range of isothermal data yielding plausible K_0, K'_0, and K'_∞ (Section IV).

The final three-parameter $P(\eta)$ fitting form is written as

$$\begin{aligned} P_{\text{macaw}}(\eta) = A\eta^{-(B+1)} \exp\left(\frac{2}{3}C\left(1-\eta^{\frac{3}{2}}\right)\right) \\ \times \left(C\eta^{\frac{3}{2}}+B\right) - A(B+C). \end{aligned} \tag{17}$$

where A, B, C are non-negative fitting parameters. Similar to K'_∞, both K_0 and K'_0 are uniquely defined in terms of A, B, C. For the three-parameter model in Eq. (17), these are given by

$$K_0 = A\left(B - \frac{1}{2}C + (B+C)^2\right), \tag{18}$$

$$K'_0 = B + C - 2 + \frac{3}{4}\left[\frac{4B(B+C+1)-C}{B-C/2+(B+C)^2}\right]. \tag{19}$$

It is also possible to invert Eq. (13), Eq. (18), and Eq. (19) to obtain A, B, C in terms of the physically meaningful K_0, K'_0, and K'_∞. The expressions are summarized in Appendix B.

B. Properties

The MACAW reference curve in Eq. (17) is a robust three-parameter functional form designed to overcome some of the deficiencies described in Section II while keeping simple analytic expressions for the free energy and sounds speeds. It satisfies the linearity constraint $K'_\infty = (P/K)_\infty$ with a material-dependent value at infinite pressures that provides additional flexibility. Similar to the Keane isotherm, the pressure function $P_{\text{macaw}}(\eta)$ becomes stiffer with increasing K'_∞ and reduces to the Murnaghan limit for $K'_\infty = K'_0$. Computing the bulk modulus from Eq. (17) yields the following expression:

$$\begin{aligned} K_{\text{macaw}}(\eta) = A\eta^{-(B+1)} \exp\left(\frac{2}{3}C\left(1-\eta^{\frac{3}{2}}\right)\right) \\ \times \left[\left(C\eta^{\frac{3}{2}}+B\right)^2 - \left(\frac{1}{2}C\eta^{\frac{3}{2}}-B\right)\right]. \end{aligned} \tag{20}$$

Eq. (20) is a strictly monotonic function with no real roots. The bulk modulus remains positive in all volume space and asymptotes to zero at infinite expansions. Therefore, the minimum pressure value $P_{\min} = -A(B+C)$ is also reached as $\eta \to \infty$. As mentioned in the introduction, this behavior is required to maintain the hyperbolicity of the governing equations under all flow conditions. The derivative of the bulk modulus with respect to pressure is also monotone for $B \geq B_{\min}$ reaching the minimum at K'_∞ as $P \to \infty$.

Stacey and Hodgkinson[21] recently suggested an additional constraint on the gradient of $(1/K')$ versus (P/K) at infinite pressures. This constraint can be written as

$$\left[\frac{\mathrm{d}(1/K')}{\mathrm{d}(P/K)}\right]_\infty = 1 - \frac{\lambda_\infty}{K'_\infty} > \frac{2}{3}\frac{f_\infty}{K'_\infty}, \tag{21}$$

where the right-hand side of the inequality arise from the restriction in Eq. (15). The three-parameter model in Eq. (17) meets this criteria for $f_\infty < 3/2(K'_\infty - 3/2)$ since Eq. (15) was utilized in the derivation. Stacey[36] includes a list of isothermal equations of state that pass and fail this test.

A shortcoming of the three-parameter MACAW with $D = 3/2$ is that any calibration with $B < B_{\min} \approx 45/29$ will have a local minimum in K' at finite compressions, i.e., $K'_\infty \neq \min(K')$. Therefore, it is recommended to constrain $B \gtrsim 45/29$ to guarantee $K'' < 0$. This imposes a lower bound on the range of permitted values for K'_∞ and the stiffness of the curve. Relaxing this constraint may occasionally lead to better fits in pressure-volume space but care should be exercised to ensure an adequate extrapolation in the compression range of interest. Recall that Birch-Murnaghan also displays a local minimum in K' for $K'_0 \in (4, 14/3)$. Convexity of the reference curve simply requires $K' > -1$ and it is guaranteed for any $B > 0$ in Eq. (17).

Other three-parameter alternatives can be constructed by replacing D in Eq. (11) with other numerical values or expressions. For instance, one could use a linear approximation of Eq. (12) such that D becomes a function of B. However, this approach leads to a bulk modulus that does not increase uniformly with B, thus two different B values will produce similar fits. We disregard this option since $P(\eta)$ should become stiffer with increasing K'_∞.

IV. CALIBRATION TO ISOTHERMAL DATA

The five functional forms given in Sections II and III are calibrated against isothermal compression data for the molecular high explosive cyclotetramethylene tetranitramine (HMX), single-crystal magnesium oxide (MgO), and two noble metals, namely gold (Au) and platinum (Pt). We employ the *basin-hopping* global optimization algorithm of Wales and Doye[37] with the implementation included in the LMFIT[38] Python package. This algorithm is noticeably slower than the more traditional Levenberg-Marquardt or Gauss-Newton methods, but it generally prevents falling into a local minimum for poor initial guesses. This is a common issue when fitting experimental pressure-volume data over small compression ratios or with significant data scatter.

The pressure residuals for each material and reference curve are shown in Fig. 5 over the compression ratio $(1/\eta)$. Table I contains the numerical value for the parameters along with the root-mean-square deviation (RMS). The values in parentheses indicate the standard deviation of the fitting parameter. This metric is not given when the value is either fixed (Birch, Vinet) or calculated using the fitting parameters (Davis, MACAW). The tabulated experimental data for the four materials can be found in pressure-volume or pressure-density format in each reference. The reference density ρ_0 is used to evaluate η and is held constant in the calibration. The parameters in Table I are obtained by fitting the nominal pressure values without accounting for the experimental uncertainty. Using a different error metric that accounts for such uncertainty will give a slightly different calibration.

To highlight certain features, some thermodynamic quanti-

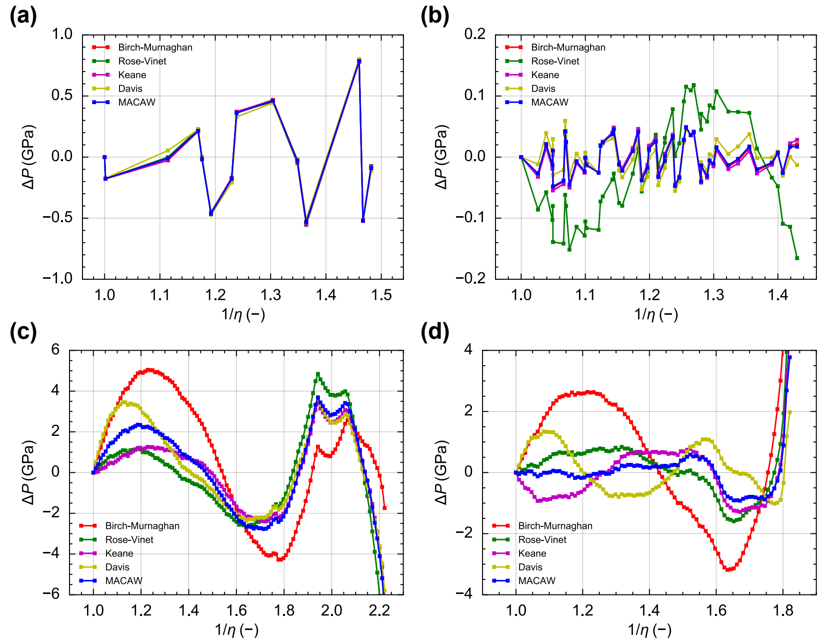

FIG. 5. Pressure residuals resulting from the nonlinear fit to isothermal compression data for (a) HMX[39], (b) MgO[40], (b) Au[41], and (c) Pt[41]

TABLE I. Parameter values and root mean square deviation in GPa for each calibration to isothermal compression data. The values in parentheses indicate the standard deviation of the fitting parameter. The reference density ρ_0 displayed in the first column corresponds to the experimental value at ambient pressure and is held constant in the calibration.

Material	Ref. Curve	A([a])	B (-)	C (-)	K_0 (GPa)	K_0' (-)	K_∞' (-)	RMS (GPa)
	Birch	-	-	-	14.56 (1.02)	8.69 (0.68)	3	0.3640
	Vinet	-	-	-	15.15 (0.75)	7.91 (0.29)	2/3	0.3639
HMX[39]	Keane	-	-	-	14.38 (3.87)	9.21 (5.15)	4.41 (1.32)	0.3642
(ρ_0=1.893 g/cm^3)	Davis	3.06 (0.37)	1.31 (0.87)	9.10 (18.07)	17.72	4.61	4	0.3622
	MACAW	0.19 (0.12)	1.63 (2.20)	7.36 (4.78)	15.22	7.54	2.63	0.3634
	Birch	-	-	-	160.27 (0.04)	4.027 (0.002)	3	0.0272
	Vinet	-	-	-	157.61 (0.15)	4.315 (0.007)	2/3	0.0834
MgO[40]	Keane	-	-	-	160.05 (0.16)	4.07 (0.02)	2.92 (0.02)	0.0281
(ρ_0=3.584 g/cm^3)	Davis	6.706 (0.003)	1.108 (0.004)	1.93 (0.03)	161.18	3.88	4	0.0276
	MACAW	6.94 (0.07)	1.75 (0.01)	3.04 (0.04)	160.40	4.00	2.75	0.0268
	Birch	-	-	-	198.18 (0.82)	4.83 (0.01)	3	3.0052
	Vinet	-	-	-	170.27 (0.59)	5.89 (0.01)	2/3	2.4267
Au[41]	Keane	-	-	-	161.19 (2.35)	7.09 (0.16)	3.11 (0.02)	1.7841
(ρ_0=19.32 g/cm^3)	Davis	3.31 (0.01)	0.880 (0.005)	10.98 (0.17)	211.85	3.09	4	2.1742
	MACAW	4.53 (0.16)	1.87 (0.03)	4.48 (0.11)	180.83	5.30	2.87	2.1734
	Birch	-	-	-	282.13 (1.30)	5.07 (0.02)	3	2.3031
	Vinet	-	-	-	260.87 (0.52)	5.818 (0.008)	2/3	1.0138
Pt[41]	Keane	-	-	-	235.74 (2.09)	7.50 (0.12)	3.02 (0.02)	0.9208
(ρ_0=21.45 g/cm^3)	Davis	3.677 (0.009)	1.08 (0.01)	7.12 (0.17)	290.10	3.79	4	0.7602
	MACAW	5.26 (0.02)	1.55 (0.00)	5.522 (0.007)	256.69	5.76	2.55	0.6451

[a] The units are (km/s) for Davis and (GPa) for MACAW

ties are plotted versus the following independent variable:

$$x := \frac{\rho}{\rho+\rho_0} \equiv \frac{V_0}{V+V_0} \equiv (1+\eta)^{-1}.$$

Using x instead of η or $1/\eta$ has the distinct advantage of displaying all volume space for $x \in [0,1]$. That is, $x = 0$ indicates infinite expansion, $x = 1$ indicates infinite compression, and $x = 1/2$ corresponds to the reference state with $\rho = \rho_0$ or $\eta = 1$. The expressions in Sections II and III can be plotted over the x plane by replacing $\eta \to (1-x)/x$.

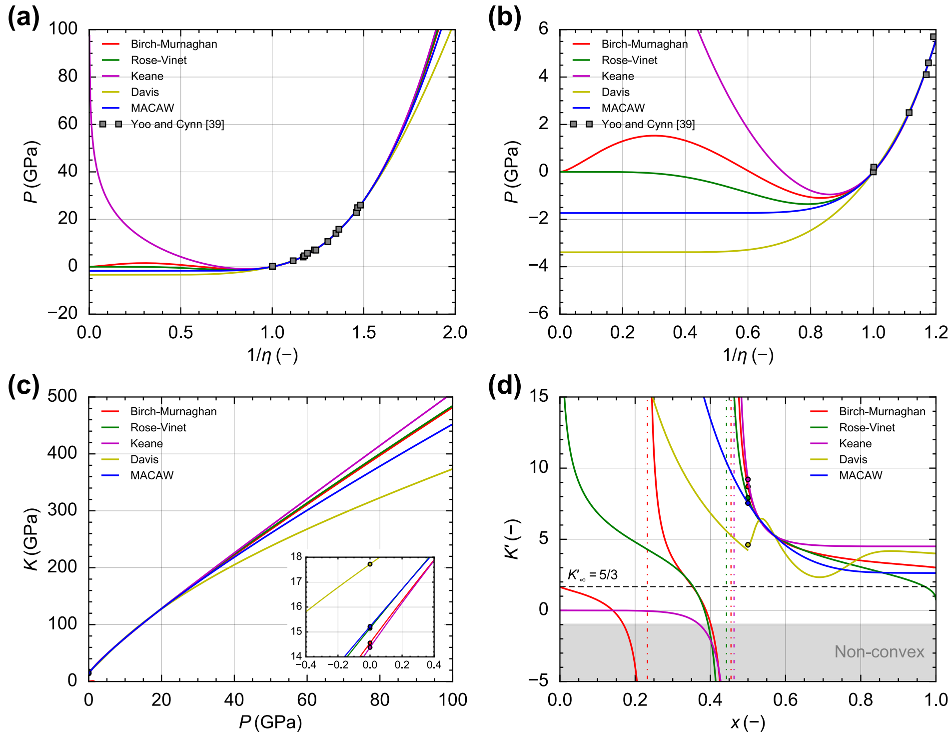

FIG. 6. Reference curve calibration to isothermal HMX data[39] in the planes (a) P-η^{-1}, (b) P-η^{-1} in expansion, (c) K-P, and (d) K'-x with $x = (1+\eta)^{-1}$. The inset in (c) shows K_0 as circular markers. The markers in (d) indicate K_0' and the dash-dotted lines are vertical asymptotes

A. Cyclotetramethylene tetranitramine (HMX)

Yoo and Cynn[39] report pressure-volume relations and vibrational Raman spectra of β-HMX obtained from diamond-anvil cell, angle-resolved synchrotron X-ray diffraction, and micro-Raman spectroscopy. Their hydrostatic data contains a kink near a pressure of 27 GPa that the authors attribute to a phase transition. It should be noted that isentropic compression experiments[42] of HMX do not reveal a phase transition at these pressures. To avoid these issues, we only utilize the Yoo-Cynn hydrostatic data below 27 GPa.

The residuals in Fig. 5(a) and RMS in Table I indicate that all five reference curves yield a similar fit over the range of data. Despite this result, the parameters for Keane, Davis, and MACAW have large relative standard deviations suggesting a fairly unconstrained optimization. Yoo and Cynn[39] report $K_0 = 12.4$ GPa and $K_0' = 10.4$ from a fit to the third-order Birch-Murnaghan below 27 GPa. These values differ considerably from those in Table I. This discrepancy in the least squares fit was already pointed out by Menikoff and Sewell[22] who obtained $K_0 = 14.7 \pm 1.3$ GPa and $K_0' = 8.6 \pm 0.8$ after accounting for the experimental uncertainty.

Fig. 6(a) depicts the five fits and data points over a wider expansion-compression range. Beyond 1.5× compression ratios, each reference curve display different degrees of stiffness with Davis being the softest and Keane the stiffest. A zoomed view into the expansion regime (Fig. 6(b)) highlights major qualitatively differences between all five isotherms. As described in Section II, the non-monotone $P(\eta)$ profile of Birch-Murnaghan, Rose-Vinet, and Keane results in a negative bulk modulus at moderate expansion ratios. Davis and MACAW differ from the rest with a strictly decreasing P as a function of η until reaching a finite $P_{\min}$. The Birch-Murnaghan contains a local maximum and a local minimum before reaching zero pressure at infinite expansion. This is due to $K_0' > 16/3$ as depicted in Fig. 1 which also translates into two vertical asymptotes in the K'-x plane. As shown in Fig. 6(d), only MACAW has a strictly monotonone K' in all volume space. Davis is also monotonically decreasing along the expansion branch, but it becomes discontinuous in K' at the reference state $x = 1/2$.

B. Magnesium oxide (MgO)

Jacobsen et al.[40] report pressure-volume data of magnesium oxide from diamond-anvil cells loaded with helium to 118 GPa. The hydrostatic data was collected using angle-dispersive, monochromatic synchrotron X-ray diffraction.

The tabulated pressure values using the MgO scale, as opposed to the ruby scale, are used to fit each of the reference isotherms at room temperature. Birch-Murnaghan, Keane, Davis, and MACAW yield similar fits as shown in Fig. 5(b) and the RMS in Table I. The RMS from Rose-Vinet is approximately three times larger than the other four functional forms with the largest discrepancy in K_0. Both Davis and Rose-Vinet also show K_0' values that deviate from typical ultrasonic and Brillouin scattering values of 4.0-4.1 in MgO[40].

Except for Rose-Vinet, Fig. 7(a) and Fig. 7(c) indicate

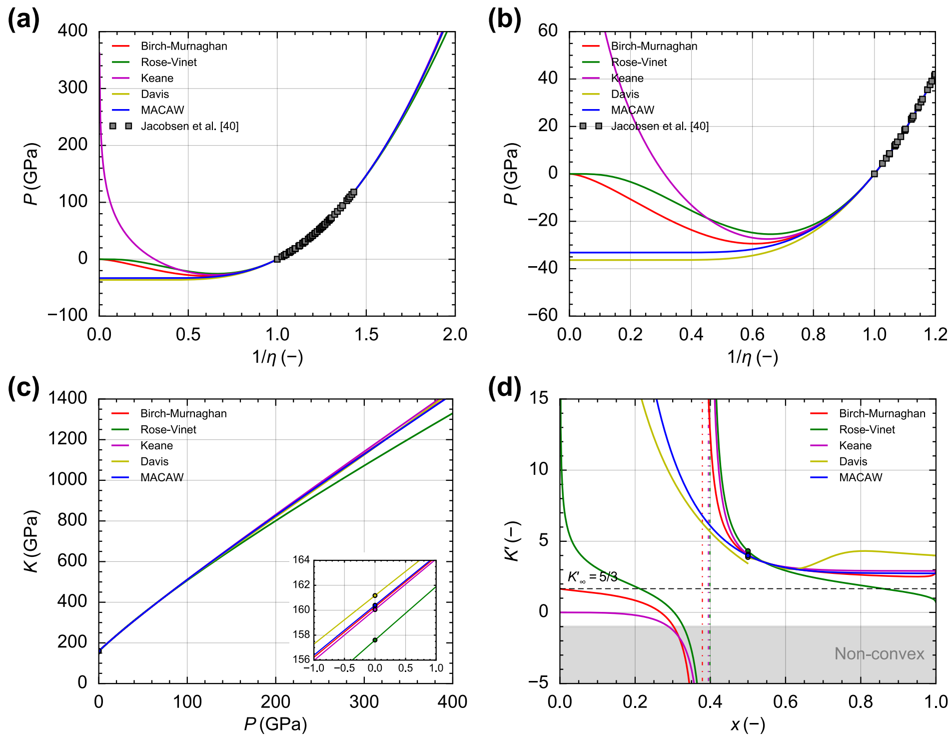

FIG. 7. Reference curve calibration to isothermal MgO data[40] in the planes (a) P-η^{-1}, (b) P-η^{-1} in expansion, (c) K-P, and (d) K'-x with $x = (1+\eta)^{-1}$. The inset in (c) shows K_0 as circular markers. The markers in (d) indicate K'_0 and the dash-dotted lines are vertical asymptotes

that the pressure and bulk modulus extrapolations from each model follow a close path in compression. In expansion, Fig. 7(b) shows that only Davis and MACAW remain monotonically decreasing. The predicted values for K_0 and K'_0 from Birch-Murnaghan, Keane, and MACAW are in close agreement. However, Fig. 7(d) reveals that the value of K'_0 for MgO results in a non-monotonic K' curve for Birch-Murnaghan in compression since $K'_0 \in (4, 14/3)$.

C. Gold (Au) and platinum (Pt)

Fratanduono et al.[41] recently reported high-pressure shockless dynamic compression results for gold and platinum collected at the National Ignition Facility and the Z machine. The authors use adiabatic ramp compression data to determine the reduced 298 K isotherm after applying a pressure correction. They report a standard deviation of 5.0% and 3.9% at 800 GPa for Au and Pt respectively, where the magnitude of the pressure correction is comparable with the experimental uncertainty[41].

Fig. 5 and Table I show the residuals and root-mean square deviation from fitting the nominal pressure values without accounting for the data uncertainty. For gold, all five residuals in Fig. 5(b) display two distinct kinks past 1.9× compression ratios with the overall best fit given by Keane. Fig. 5(c) for platinum shows a more uniform residual distribution with MACAW yielding the lowest root-mean square deviation. Table I for Pt also show a zero standard deviation for the parameter B in MACAW. This indicates that B is being forced to its prescribed lower bound 45/29 and that the best fit occurs for even lower values—specifically $B = 1.488$ gives $\mathrm{RMS} = 0.6108$. We discard any $B < 45/29$ based on the analysis in Section III A.

Fig. 8 and Fig. 9 display similar qualitative features to the HMX and MgO fits where MACAW is strictly monotonic in P, K, and K'. The Birch-Murnaghan isotherm only contains a local minimum in P-η^{-1} space due to $K'_0 < 16/3$, thus a single vertical asymptote in K'. Regarding K_0 and K'_0, both MACAW and Rose-Vinet yield similar values for all three materials versus Keane and Davis.

V. SUMMARY AND CONCLUSIONS

Most analytic isothermal models lead to numerical problems in expansion due to negative bulk modulus or are defined by piecewise functions with multiple branches. We briefly summarize the main features of four commonly-used reference curves, namely third-order Birch-Murnaghan, Rose-Vinet, Keane, and Davis. After identifying some of their advantages and deficiencies, we design a robust non-piecewise functional form with enough flexibility to fit high-pressure isothermal data and well-behaved in all volume space. The MACAW reference curve is a three-parameter form with a concave-downwards K-P relation that satisfies the linearity condition at infinite pressures. The three fitting parameters A, B, C are related to the physically-meaningful K_0, K'_0, K'_∞

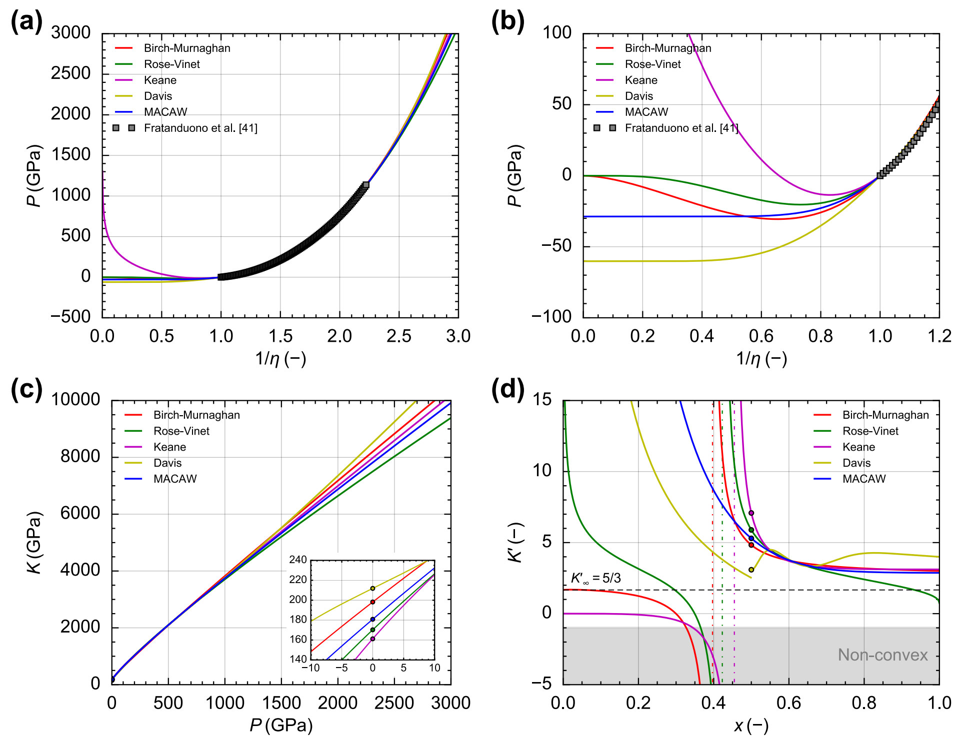

FIG. 8. Reference curve calibration to isothermal gold data[41] in the planes (a) P-η^{-1}, (b) P-η^{-1} in expansion, (c) K-P, and (d) K'-x with $x = (1+\eta)^{-1}$. The inset in (c) shows K_0 as circular markers. The markers in (d) indicate K_0' and the dash-dotted lines are vertical asymptotes

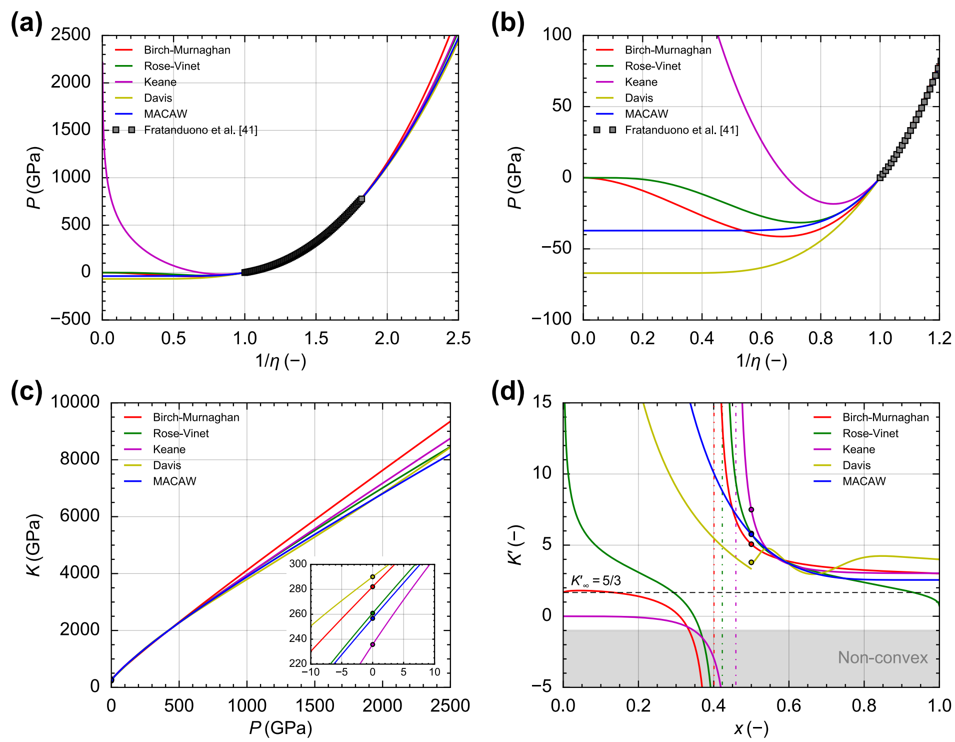

FIG. 9. Reference curve calibration to isothermal platinum data[41] in the planes (a) P-η^{-1}, (b) P-η^{-1} in expansion, (c) K-P, and (d) K'-x with $x = (1+\eta)^{-1}$. The inset in (c) shows K_0 as circular markers. The markers in (d) indicate K_0' and the dash-dotted lines are vertical asymptotes

and the Helmholtz free energy along the cold curve can be written analytically. A shortcoming of the present model is that there is a minimum value allowed for K'_∞ that guarantees $K'' < 0$. Enforcing this lower bound limits how soft the curve can become for a particular calibration. Each of the five functional forms are fitted to experimental isothermal data at room temperature for HMX, magnesium oxide, gold, and platinum using the nominal pressure values. MACAW is able to fit the data adequately with similar residuals to Keane and Davis and K_0, K'_0 values close to those of Birch-Murnaghan and Rose-Vinet. This reference curve is part of a new thermodynamically consistent and complete equation of state currently being develop to model high-explosive reactants. Future work will include calibrating MACAW to Density Functional Theory (DFT) results for multiple condensed-phase explosives.

Appendix A: Derivatives of bulk modulus and convexity

The isothermal and isentropic bulk modulus is defined as

$$K = -V \frac{\partial P}{\partial V}\bigg|_{T,S} \equiv -\eta \frac{\partial P}{\partial \eta}\bigg|_{T,S}, \tag{A1}$$

where $\eta = V/V_0$ and V_0 is the reference specific volume. Assuming a reference curve $P(V)$ or a complete EOS $P(V,T)$, we can differentiate Eq. A1 with respect to pressure by applying the chain rule:

$$\begin{aligned} K' &= \frac{\partial K}{\partial P}\bigg|_{T,S} \\ &= \frac{V_0}{V_0}\frac{\partial K}{\partial V}\bigg|_{T,S}\frac{\partial V}{\partial P}\bigg|_{T,S} \\ &= \frac{\partial K}{\partial \eta}\bigg|_{T,S}\left(\frac{\partial P}{\partial \eta}\bigg|_{T,S}\right)^{-1}. \end{aligned} \tag{A2}$$

Using the definition of the bulk modulus, K' can be rewritten in terms of K as

$$K' = -\frac{\eta}{K}\frac{\partial K}{\partial \eta}\bigg|_{T,S}, \tag{A3}$$

or alternatively in terms of P as

$$K' = -1 - \eta \frac{\partial^2 P}{\partial \eta^2}\bigg|_{T,S}\left(\frac{\partial P}{\partial \eta}\bigg|_{T,S}\right)^{-1}. \tag{A4}$$

Applying the same steps to K' yield an expression for the second derivative of the bulk modulus with respect to pressure,

$$K'' = -\frac{\eta}{K}\frac{\partial K'}{\partial \eta}\bigg|_{T,S}. \tag{A5}$$

All three quantities—K, K', K''—can be obtained analytically for the each of the $P(\eta)$ reference curves described in this paper. The bulk modulus K has units of pressure, K' is dimensionless, and K'' has units of inverse of pressure.

The expressions in Eq. (A1), Eq. (A3), and Eq. (A5) are general thermodynamic definitions and the derivation steps apply to both isothermal and isentropic bulk moduli. The convexity property of an equation of state is determined by the sign of the fundamental derivative[43],

$$\mathscr{G} = \frac{1}{2}\frac{V^3}{c^2}\frac{\partial^2 P}{\partial V^2}\bigg|_S, \tag{A6}$$

which determines the variation of the characteristic velocity along a rarefaction wave[1]. If $\mathscr{G} > 0$, the EOS is called convex with compressive shocks and expansive rarefaction waves. Since $K_S = c^2/V$, the square of the isentropic sound speed is given by

$$c^2 = -V^2 \frac{\partial P}{\partial V}\bigg|_S. \tag{A7}$$

Substituting Eq. (A7) in Eq. (A6) and $V = V_0\eta$ yields,

$$\mathscr{G} = -\frac{1}{2}\eta \frac{\partial^2 P}{\partial \eta^2}\bigg|_S \left(\frac{\partial P}{\partial \eta}\bigg|_S\right)^{-1}. \tag{A8}$$

Replacing the above expression in Eq. (A4) results in the following identity for the pressure derivative of the isentropic bulk modulus:

$$K'_S = 2\mathscr{G} - 1. \tag{A9}$$

Therefore, a convex equation of state requires $K'_S > -1$. Since the isentrope and the isotherm are coincident at T=0, this condition can be generalized to $K' > -1$ for the cold curve. Menikoff and Plohr[44] summarizes the properties of the Riemann problem and the implications for numerical algorithms when the convexity condition is violated. An anomalous wave structure caused by kinks or a smooth loss of convexity often occurs near phase transitions—see for instance in the van der Waals EOS near the vapor dome[45].

Appendix B: MACAW parameters

This appendix gives the A, B, C parameters in Eq. (17) in terms of K_0, K'_0, and K'_∞. Solving for C using the expression for K'_0 results in one real root and two complex conjugates. The real root is the only one with physical relevance and can be expressed as:

$$C = \frac{11}{6} + \frac{1}{3}K'_0 - K'_\infty + \frac{2^{-\frac{1}{3}}}{6}\omega + \frac{2^{\frac{1}{3}}}{3}\left(\frac{b}{\omega}\right), \tag{B1}$$

where,

$$\begin{aligned} \omega &= \left(a + \sqrt{a^2 - 32b^3}\right)^{1/3}, \\ a &= 16(K'_0)^3 + 84(K'_0)^2 + 192K'_0 - 972K'_\infty + 1177, \\ b &= 2(K'_0)^2 + 7K'_0 - 27K'_\infty + 38. \end{aligned}$$

From Eq. (13), B is simply given by:

$$B = K'_{\infty} - 1. \tag{B2}$$

Finally, A can be computed using the values of B, C, and K_0:

$$A = K_0 \left(B - \frac{1}{2}C + (B+C)^2 \right)^{-1}. \tag{B3}$$

ACKNOWLEDGMENTS

The authors would like to thank Marc Cawkwell, Jeff Leiding, Ralph Menikoff, D.J. Luscher, Dan Hooks and Nick Whitworth for many insightful discussions. This research was supported by the Advanced Simulation and Computing Program (ASC) at Los Alamos National Laboratory under Contract No. 89233218CNA000001. T.D.A. also acknowledges funding from Dan Borovina through the LANL "CHE Grand Challenge" Project.

AUTHOR DECLARATIONS

Conflict of Interests

The authors have no conflicts to disclose.

DATA AVAILABILITY STATEMENT

The data that support the findings of this study are openly available in references[39–41].

REFERENCES

[1] R. Menikoff, in *ShockWave Science and Technology Reference Library* (Springer, 2007) pp. 143–188.
[2] M. J. Cawkwell, M. Zecevic, D. J. Luscher, and K. J. Ramos, Propellants, Explosives, Pyrotechnics **46**, 705 (2021).
[3] P. B. Roy and S. B. Roy, Journal of Physics: Condensed Matter **17**, 6193 (2005).
[4] F. Birch, Physical Review **71**, 809 (1947).
[5] P. Vinet, J. H. Rose, J. Ferrante, and J. R. Smith, Journal of Physics: Condensed Matter **1**, 1941 (1989).
[6] A. Keane, Australian Journal of Physics **7**, 322 (1954).
[7] A. Rajendran, M. Dietenberger, and D. Grove, Journal of Applied Physics **65**, 1521 (1989).
[8] F. Addessio and J. Johnson, Journal of Applied Physics **74**, 1640 (1993).
[9] B. Wescott, D. S. Stewart, and W. C. Davis, Journal of Applied Physics **98**, 053514 (2005).
[10] T. D. Aslam, Journal of Applied Physics **123**, 145901 (2018).
[11] W. C. Davis, Combustion and Flame **120**, 399 (2000).
[12] D. S. Stewart, S. Yoo, and W. C. Davis, in *12th Symp.(Intl) on Detonation* (2002) pp. 1–11.
[13] T. D. Aslam, Journal of Applied Physics **122**, 035902 (2017).
[14] N. Whitworth and B. Lambourn, AIP Conference Proceedings **1979**, 030007 (2018).
[15] R. S. Menikoff, *Complete EOS for PBX 9502*, Tech. Rep. LA-UR-09-06529 (Los Alamos National Laboratory, 2009).
[16] K. A. Velizhanin and J. D. Coe, AIP Conference Proceedings **2272**, 070051 (2020).
[17] F. Stacey, B. Brennan, and R. Irvine, Geophysical Surveys **4**, 189 (1981).
[18] W. M. Elsasser, Science **113**, 105 (1951).
[19] W. Holzapfel, Reports on Progress in Physics **59**, 29 (1996).
[20] F. Stacey and P. Davis, Physics of the Earth and Planetary Interiors **142**, 137 (2004).
[21] F. D. Stacey and J. H. Hodgkinson, Physics of the Earth and Planetary Interiors **286**, 42 (2019).
[22] R. Menikoff and T. D. Sewell, International Journal of High Pressure Research **21**, 121 (2001).
[23] J. H. Rose, J. R. Smith, and J. Ferrante, Physical Review B **28**, 1835 (1983).
[24] P. Vinet, J. Ferrante, J. H. Rose, and J. R. Smith, Journal of Geophysical Research: Solid Earth **92**, 9319 (1987).
[25] P. M. Morse, Physical Review **34**, 57 (1929).
[26] R. Rydberg, Zeitschrift für Physik **73**, 376 (1932).
[27] J. Hama and K. Suito, Journal of Physics: Condensed Matter **8**, 67 (1996).
[28] W. B. Holzapfel, International Journal of High Pressure Research **16**, 81 (1998).
[29] F. D. Murnaghan, Proceedings of the National Academy of Sciences **30**, 244 (1944).
[30] R. Fürth, Proceedings of the Royal Society of London. Series A. Mathematical and Physical Sciences **183**, 87 (1944).
[31] F. D. Stacey, Geophysical Journal International **143**, 621 (2000).
[32] J. W. Enig, Journal of Applied Physics **34**, 746 (1963).
[33] W. C. Davis, in *Explosive Effects and Applications* (Springer, 1998) pp. 47–113.
[34] J. M. Walsh and R. H. Christian, Physical Review **97**, 1544 (1955).
[35] O. Anderson, *Equations of State for Solids in Geophysics and Ceramic Science*, Vol. 31 (Oxford University Press, 1995).
[36] F. D. Stacey, Minerals **9**, 636 (2019).
[37] D. J. Wales and J. P. Doye, The Journal of Physical Chemistry A **101**, 5111 (1997).
[38] M. Newville, T. Stensitzki, D. B. Allen, and A. Ingargiola, LMFIT: Non-Linear Least-Square Minimization and Curve-Fitting for Python (2014).
[39] C.-S. Yoo and H. Cynn, The Journal of Chemical Physics **111**, 10229 (1999).
[40] S. D. Jacobsen, C. M. Holl, K. A. Adams, R. A. Fischer, E. S. Martin, C. R. Bina, J.-F. Lin, V. B. Prakapenka, A. Kubo, and P. Dera, American Mineralogist **93**, 1823 (2008).
[41] D. E. Fratanduono, M. Millot, D. G. Braun, S. J. Ali, A. Fernandez-Pañella, C. T. Seagle, J.-P. Davis, J. L. Brown, Y. Akahama, R. G. Kraus, M. C. Marshall, R. F. Smith, E. F. O'Bannon, J. M. McNaney, and J. H. Eggert, Science **372**, 1063 (2021).
[42] D. E. Hooks, D. B. Hayes, D. E. Hare, D. B. Reisman, K. S. Vandersall, J. W. Forbes, and C. A. Hall, Journal of Applied Physics **99**, 124901 (2006).
[43] P. A. Thompson, The Physics of Fluids **14**, 1843 (1971).
[44] R. Menikoff and B. J. Plohr, Reviews of Modern Physics **61**, 75 (1989).
[45] M. S. Cramer and R. Sen, The Physics of Fluids **30**, 377 (1987).

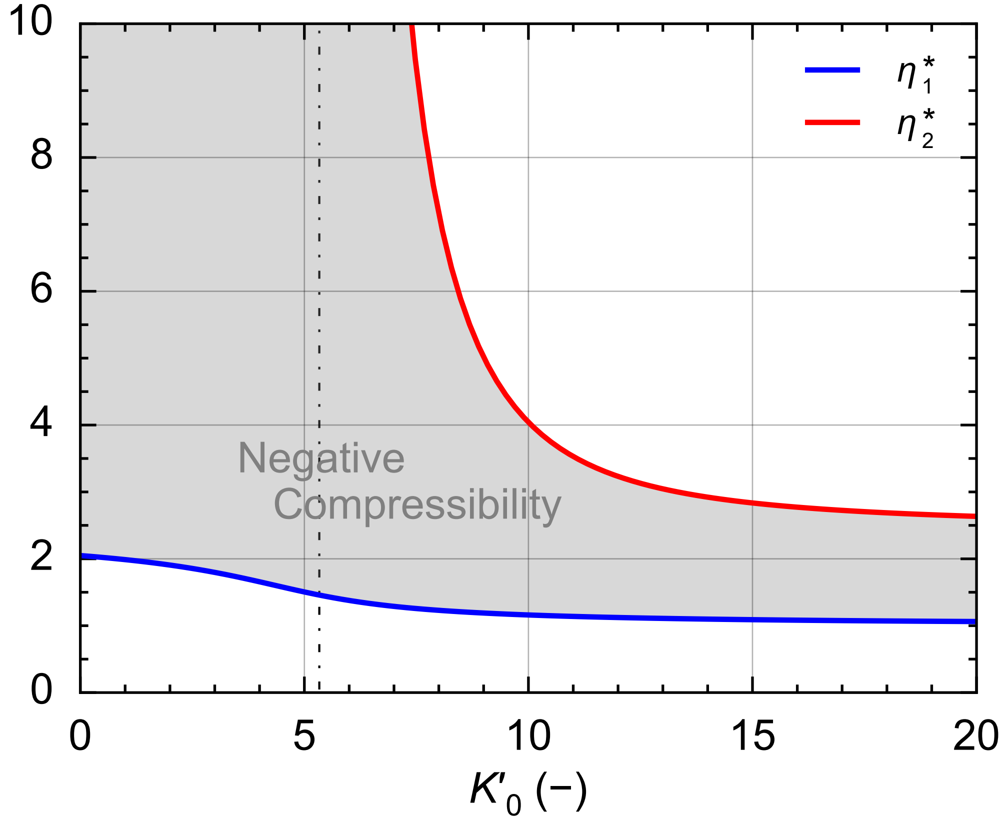
η^* (−)
K'_0 (−)
η_1^*
η_2^*
Negative Compressibility
0
2
4
6
8
10
0
5
10
15
20

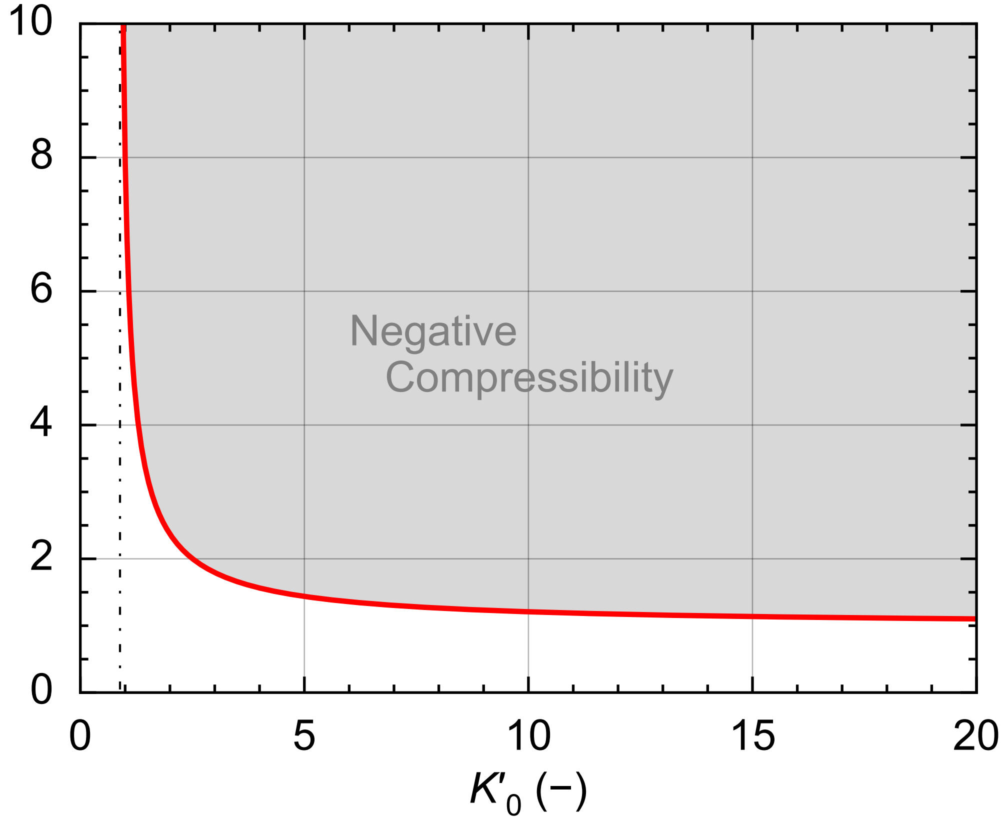

Negative
Compressibility
η* (−)
K'0 (−)
0
2
4
6
8
10
0
5
10
15
20

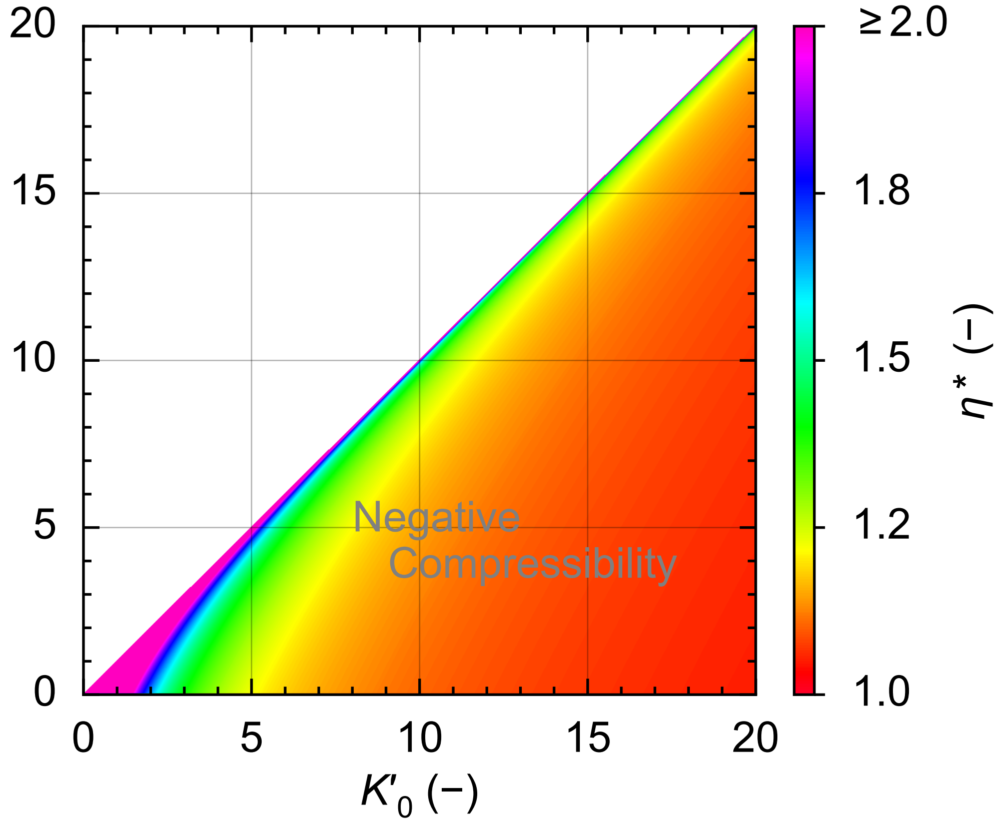
Negative
Compressibility
K′∞ (−)
K′0 (−)
η* (−)
≥2.0
1.8
1.5
1.2
1.0
0
5
10
15
20

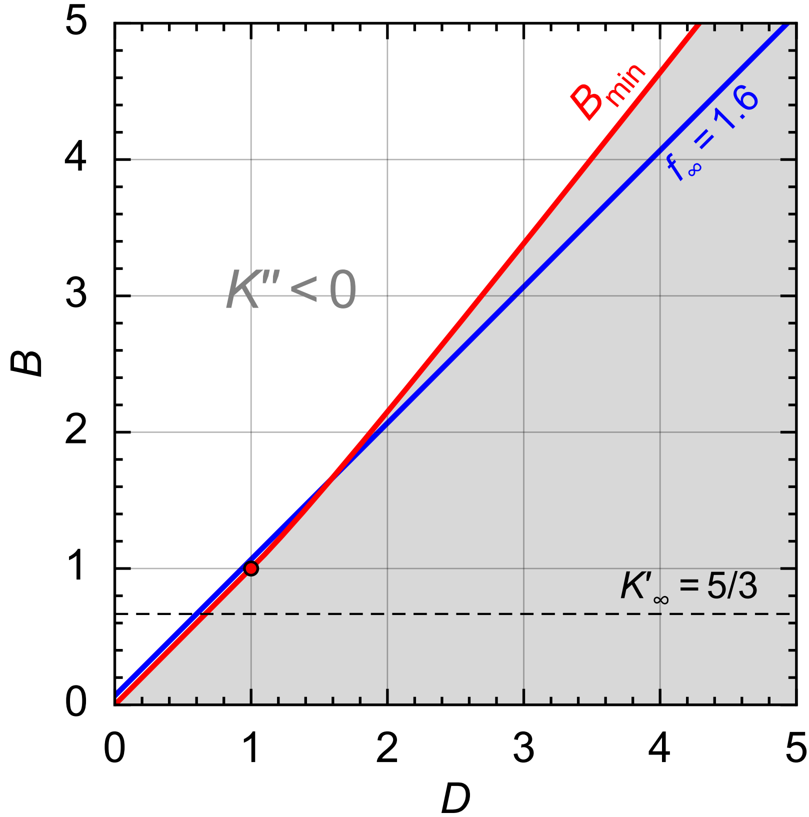
B
D
$K'' < 0$
B_{min}
$f_\infty = 1.6$
$K'_\infty = 5/3$
0
1
2
3
4
5

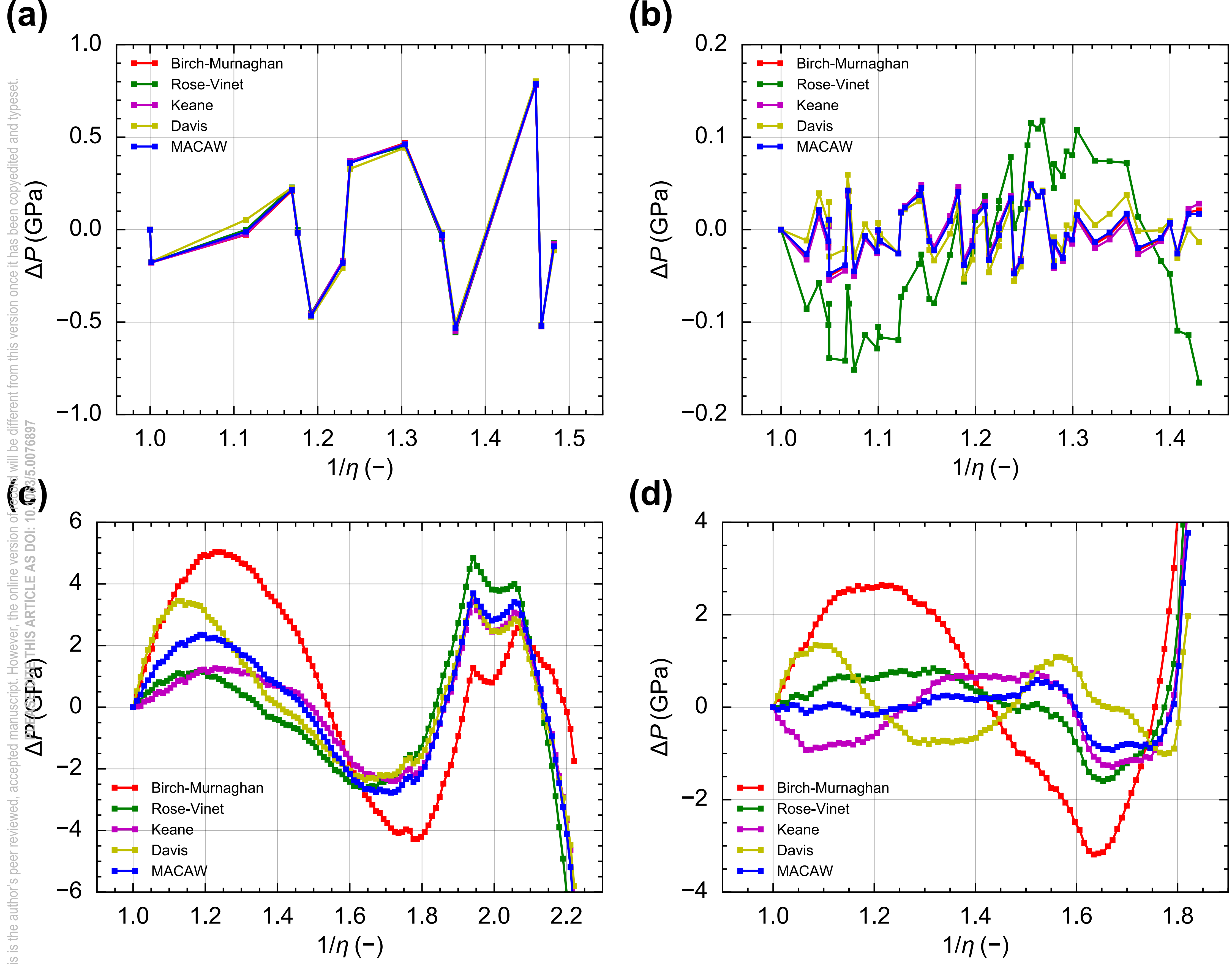
(a)
(b)
(c)
(d)
Birch-Murnaghan
Rose-Vinet
Keane
Davis
MACAW
ΔP (GPa)
1/η (−)

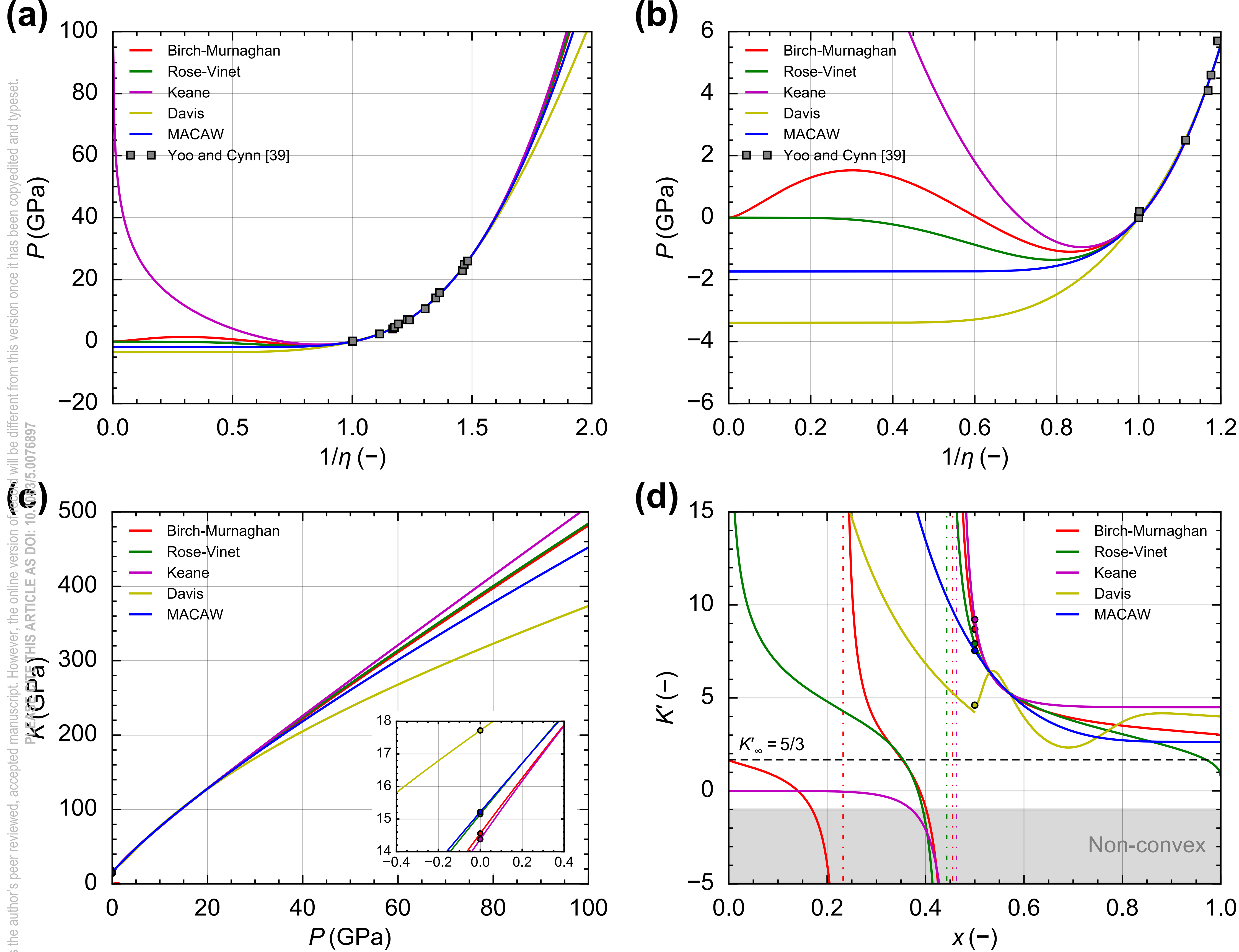
(a)
Birch-Murnaghan
Rose-Vinet
Keane
Davis
MACAW
Yoo and Cynn [39]
P (GPa)
1/η (−)
(b)
Birch-Murnaghan
Rose-Vinet
Keane
Davis
MACAW
Yoo and Cynn [39]
P (GPa)
1/η (−)
(c)
Birch-Murnaghan
Rose-Vinet
Keane
Davis
MACAW
K (GPa)
P (GPa)
(d)
Birch-Murnaghan
Rose-Vinet
Keane
Davis
MACAW
K′∞ = 5/3
Non-convex
K′ (−)
x (−)

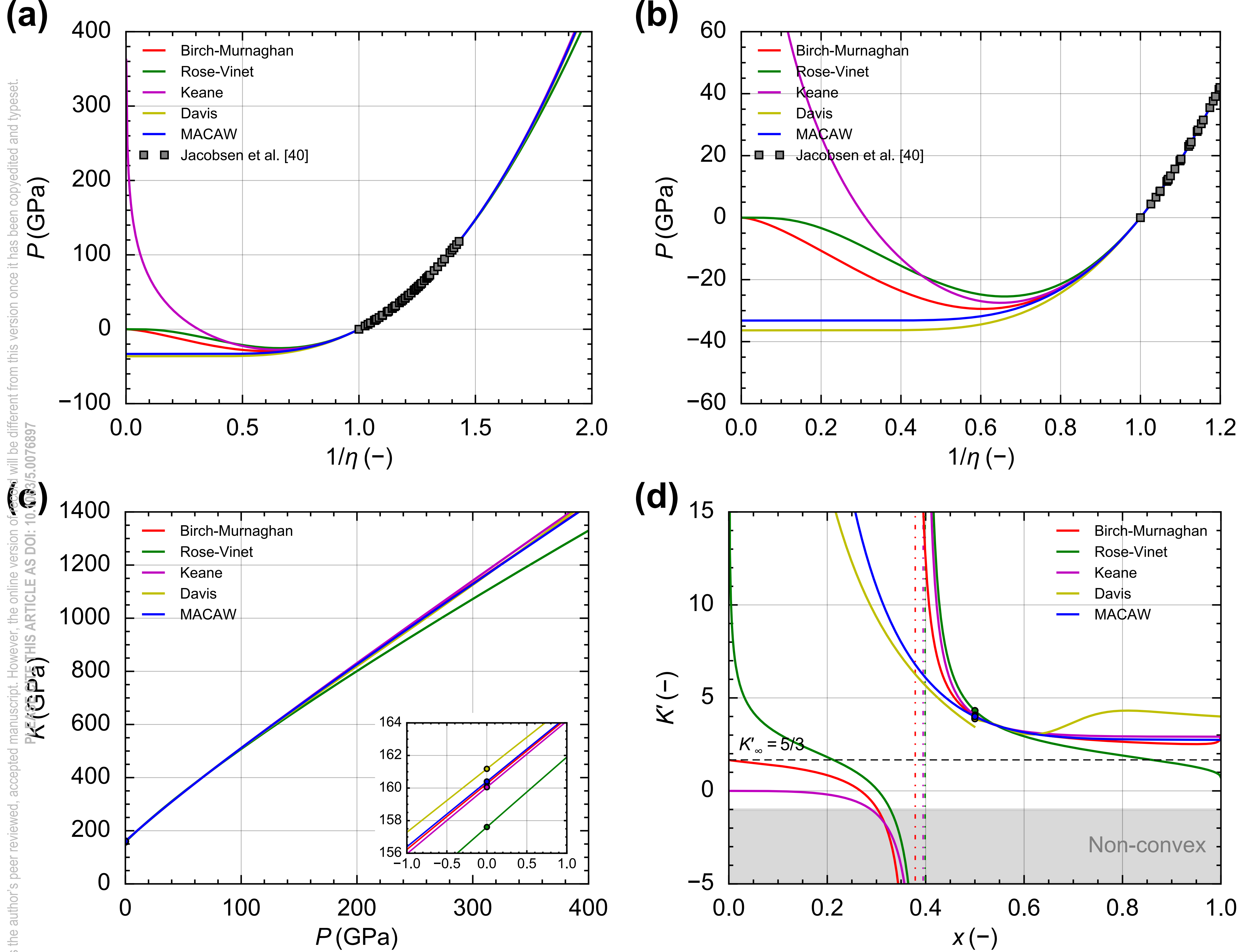
(a)
(b)
(c)
(d)
Birch-Murnaghan
Rose-Vinet
Keane
Davis
MACAW
Jacobsen et al. [40]
P (GPa)
$1/\eta$ (−)
K (GPa)
P (GPa)
K' (−)
x (−)
$K'_\infty = 5/3$
Non-convex

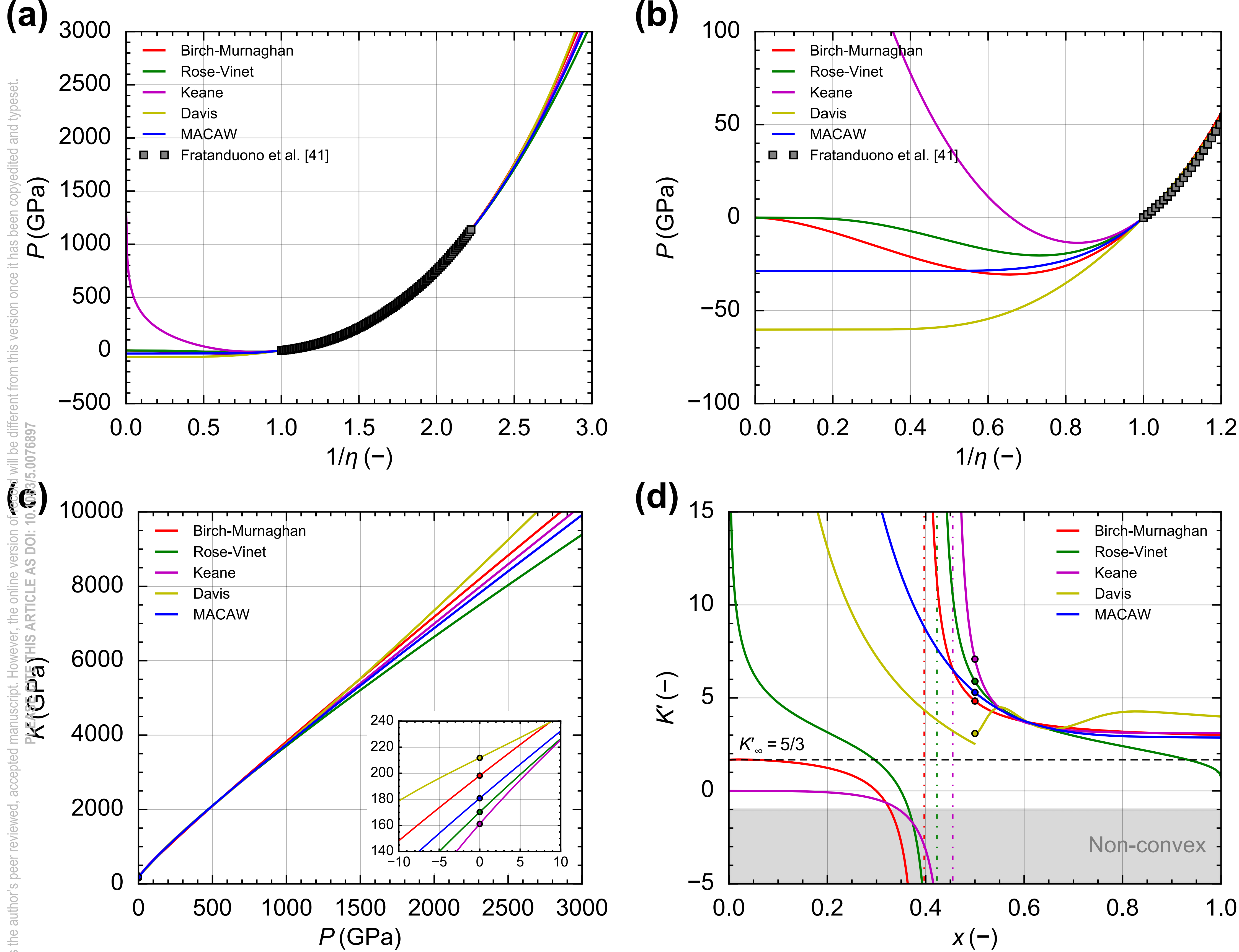
(a)
(b)
(c)
(d)
Birch-Murnaghan
Rose-Vinet
Keane
Davis
MACAW
Fratanduono et al. [41]
P (GPa)
1/η (−)
K (GPa)
K′ (−)
x (−)
K′∞ = 5/3
Non-convex

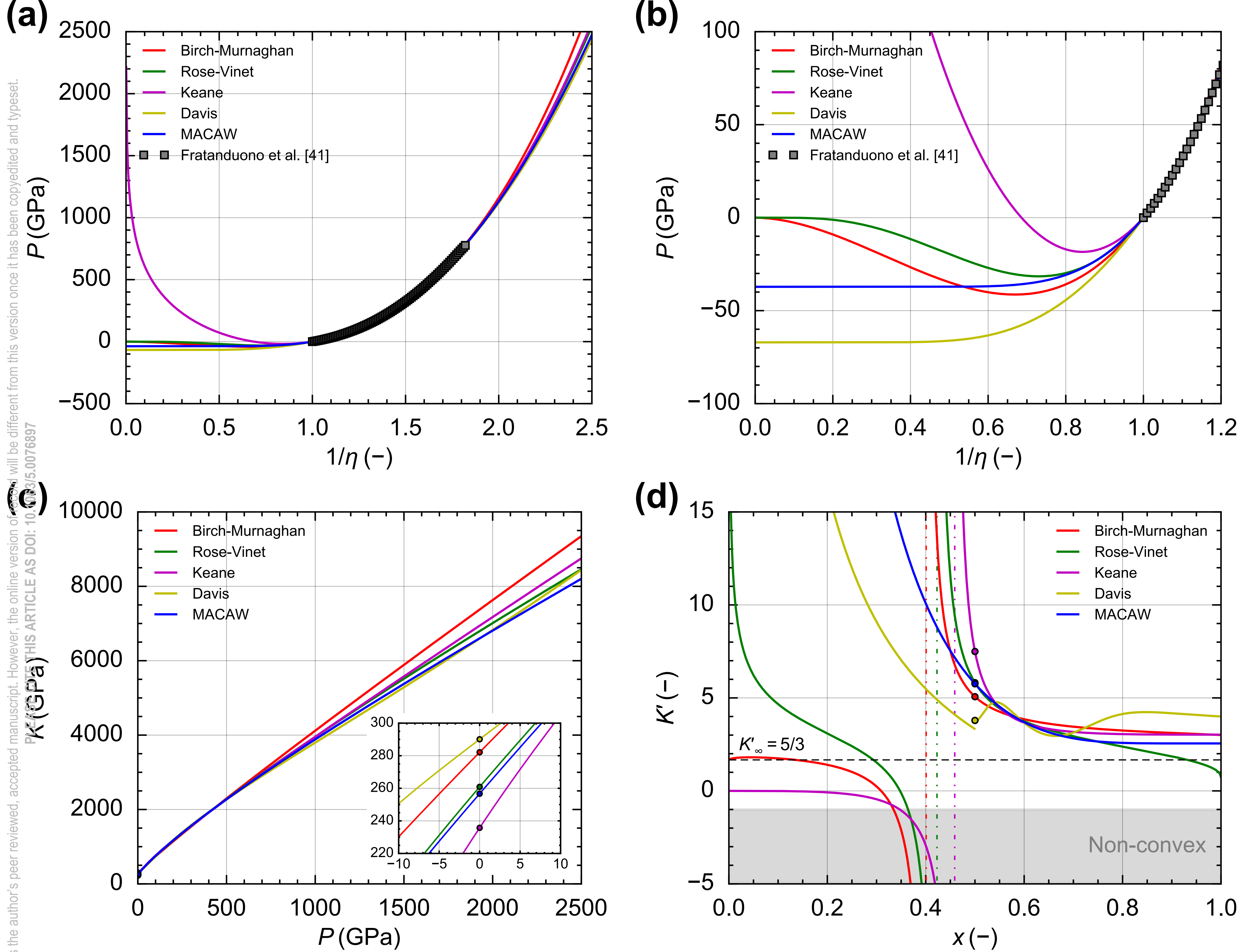
(a)
P (GPa)
1/η (−)
Birch-Murnaghan
Rose-Vinet
Keane
Davis
MACAW
Fratanduono et al. [41]
(b)
P (GPa)
1/η (−)
Birch-Murnaghan
Rose-Vinet
Keane
Davis
MACAW
Fratanduono et al. [41]
(c)
K (GPa)
P (GPa)
Birch-Murnaghan
Rose-Vinet
Keane
Davis
MACAW
(d)
K′ (−)
x (−)
Birch-Murnaghan
Rose-Vinet
Keane
Davis
MACAW
K′∞ = 5/3
Non-convex